Equation of state and collision rate tests of parton cascade models

Bin Zhang,[1] Miklos Gyulassy,[1] and Yang Pang[1,2]
[1]*Physics Department, Columbia University, New York, New York 10027*
[2]*Brookhaven National Laboratory, Upton, New York 11973*
(Received 20 January 1998)

We develop two further numerical tests of parton cascade models: the ideal gas equation of state and the collision frequency tests. The equation of state test checks the initial momentum distribution generator and free expansion dynamics in periodic inhomogeneous geometries. The collision rate test is sensitive to spatial inhomogeneities and the collision algorithm. These tests are applied to the recently developed ZPC parton cascade model. The tests helped uncover unphysical correlations induced by one of the commonly used random number generators and showed the necessity of particle subdivisions for convergence to the exact analytic limit. [S0556-2813(98)06508-5]

PACS number(s): 25.75.−q, 21.65.+f, 24.10.Jv, 24.10.Lx

I. INTRODUCTION

Many observables in nuclear collisions are difficult to calculate analytically because the number of particles is neither large enough to justify rigorously the application of statistical mechanics nor small enough to justify impulse approximations. In most cases, numerical simulations of transport equations are required to compare theory with experiment. However, due to the complexity of the algorithms employed and the number of untested dynamical assumptions [1–4], it is not straightforward to check or even reproduce the numerical results from parton cascade codes. Recently, several analytic tests were proposed to help check the accuracy and identify limitations of such codes. In the context of earlier nonrelativistic transport models tests such as comparing with the analytic Krook-Wu model [5] have been useful. In the context of hydrodynamics, numerical hydrodynamic codes have been tested in cases of expansion of baryon free matter into vacuum [6] and ''slab-on-slab'' collision [7].

To address the new generation of parton cascade codes, an Open Standard for Codes and Routines (OSCAR) [8] has been developed to enable objective testing of essential components of algorithms and ensure reproducibility of numerical results. In this context, we have proposed in Ref. [9] a dynamical test of the evolution of the transverse energy in $1+1$ dimensional expansion for cascade models. Another test of the frame and scattering scheme dependence of cascade models was proposed in [10,11]. In this paper, we propose two further tests for the OSCAR standard: the equation of state and the collision rate test of one-component relativistic classical gases.

The tests provide information about the nature of the code's initial momentum distribution and check its evolution algorithm in free expansion in periodic spatial inhomogeneities against nontrivial analytic expressions. The transverse to parallel momentum flux ratio tests the evolution of space-time and momentum space correlations. The asymptotic homogeneous equilibrated state tests the equation of state of the model against the expected ideal gas laws. The collision frequency test checks the basic collision algorithm.

We apply these tests to the recently developed ZPC parton cascade model [4]. In order to pass these tests, we uncovered and fixed a problem with one of the random number generators used in ZPC. We discuss that example in detail to illustrate the importance of applying such numerical tests. We propose to add these tests to the group already in the OSCAR standard [8].

The paper is organized as follows: In Sec. II, we recall basic statistical mechanics relations of ideal gas and calculate the free streaming evolution of periodic slab initial spatial distribution. In addition the collision rate is discussed. Numerical tests of ZPC are compared to analytical predictions in Sec. III. We conclude by emphasizing the importance of testing cascade codes.

II. ANALYTIC TESTS

A. Equation of state

The partition function for an ideal relativistic classical gas with mass m and degeneracy γ is given by [12] ($\hbar=c=k_B=1$)

$$Z(N,T,V)=\frac{1}{N!}\left(\frac{\gamma V}{2\pi^2}(Tm^2)K_2(m/T)e^{m/T}\right)^N. \tag{1}$$

In the $N\gg 1$ limit, the free energy, $F=-T\ln Z$ is well approximated by

$$F(N,T,V)=-N\left[T\ln\left(\frac{\gamma}{2\pi^2}\frac{VTm^2}{N}K_2(m/T)\right)+m+T\right]. \tag{2}$$

The pressure, $P=-\partial F/\partial V$ is given by the well-known ideal-gas law

$$P(N,T,V)=\rho T, \tag{3}$$

in terms of the density $\rho=N/V$, and the energy density is given by

$$\epsilon(N,T,V)=\rho m[K_1(\beta m)/K_2(\beta m)+3T/m], \tag{4}$$

where $\beta=1/T$. For fixed N,V an interesting quantity that reflects the softness of the equation of state is

 © 1998 The American Physical Society

$$\frac{P}{\epsilon}=\frac{1}{3+\beta m K_1(\beta m)/K_2(\beta m)}. \tag{5}$$

In the $m/T \ll 1$ relativistic limit, $P/\epsilon \approx 1/3$, while in the nonrelativistic limit, $P/\epsilon \approx T/m$.

In a cascade simulation, these thermodynamic quantities can be measured as a function of time by computing the spatially averaged energy-momentum tensor

$$\langle T^{\mu\nu}\rangle = \frac{1}{V}\sum_i \frac{p_i^\mu p_i^\nu}{E_i}. \tag{6}$$

Then $\epsilon = \langle T^{00}\rangle$ and $P=\langle T^{11}\rangle$. In Sec. III, we will compare the analytic results of the pressure-energy density ratio as a function of m/T, and the energy density as a function of T.

B. Free expansion in slab geometries

A simple test of equilibration in a *periodic* box of volume $V=L^3$ and fixed particle number is provided by taking the initial spatial distribution to be confined to one half of the box (say with $x>0$):

$$f(x,p,0)=\rho_0\left(1+\frac{4}{\pi}\,\mathrm{Im}\,\tanh^{-1}[e^{2\pi i x/L}]\right)f(p). \tag{7}$$

In the above, $\rho_0 = N/V$ is the equilibrium particle density, L is the length of the box, and

$$f(p)=\frac{\exp(-\beta\sqrt{m^2+p^2})}{4\pi(m^2/\beta)K_2(\beta m)}. \tag{8}$$

For the free streaming case, $f(\vec{x},\vec{p},t)=f(\vec{x}-\vec{p}t/p^0,\vec{p},0)$.

For the interesting case of massless partons, the momentum flux component, T^{11} evolves from its initial value

$$T^{11}(x,0)=T^{11}(\infty)\left(1+\frac{4}{\pi}\,\mathrm{Im}\,\tanh^{-1}[e^{2\pi i x/L}]\right), \tag{9}$$

to its final value $T^{11}(\infty)=\rho_0\int d^3p\, p_x^2/p^0 f(p)$ via

$$\frac{T^{11}(x,t)}{T^{11}(\infty)}=1+\frac{a}{t^3}\sum_{l=0}^{\infty}\frac{\sin(k_n x)}{n^4}\times\{[(k_n t)^2-2]\sin(k_n t)+2k_n t\,\cos(k_n t)\}. \tag{10}$$

Here $a=3L^3/(2\pi^4)$, $n=2l+1$, and $k_n=2\pi n/L$. The infinite sum can be expressed in terms of the Lerch $\Phi(z,n,a)$ functions, but in practice the series converges very rapidly. For example the evolution at the ''midway'' points $x=(2k+1)L/4$ involves damped oscillations with maxima and minima occurring at times $t=(2m+1)L/4$. At $x=L/4$, the ''11'' momentum flux oscillates within the envelopes

$$T^{11}(x=L/4,0)=T^{11}(\infty)\left[1\pm\frac{\epsilon}{4}\left(\frac{3L}{t}-\frac{L^3}{8t^3}\right)\right] \tag{11}$$

reaching the envelope at times $t=(2m+1)L/4$. Note that free streaming in this geometry leads to global homogeneous equilibrium through mixing from neighboring slabs. The deviation of the parton cascade evolution from this result when collisions terms are turned on are of physical interest as tests of collective hydrodynamic behavior.

Another interesting probe of the evolution is the transverse-longitudinal momentum flux anisotropy,

$$A^{zx}(x,t)\equiv\langle T^{33}(x,t)\rangle/\langle T^{11}(x,t)\rangle. \tag{12}$$

Initially, in the $-L/2<x<0$ region we set $A^{zx}=0$, while in the $0<x<L/2$ region $A^{zx}=1$. In the case of free streaming, this anisotropy is given by

$$A^{zx}(x,t)=\frac{1+(a/t^3)\sum_{l=0}^{\infty}[\sin(k_n x)/n^4][\sin(k_n t)-k_n t\,\cos(k_n t)]}{1+(a/t^3)\sum_{l=0}^{\infty}[\sin(k_n x)/n^4]\{[(k_n t)^2-2]\sin(k_n t)+2\,k_n t\,\cos(k_n t)\}}. \tag{13}$$

We note that of course other nonequilibrium initial conditions, e.g., homogeneous spatial distribution with anisotropic momentum distribution, can be set up to test dynamical relaxation toward global equilibrium. In this paper we will study only the evolution of spatial inhomogeneous conditions.

C. Collision rate for an isotropic, homogeneous gas

The collision rate per unit volume W is another quantity that can be easily monitored. It is related to the number of collisions N_c in a period of time t via

$$W=\frac{N_c}{Vt}. \tag{14}$$

We take the integrated parton elastic cross section to be

$$\sigma_{gg\to gg}=\frac{\pi}{\mu^2}. \tag{15}$$

The total collision rate per unit volume can be calculated from

$$W=\langle\sigma\rho_1\rho_2|\vec{v}_1-\vec{v}_2|\rangle$$
$$=\frac{1}{2}\frac{\pi}{\mu^2}\gamma^2\int\frac{d^3p_1}{(2\pi)^3}\frac{d^3p_2}{(2\pi)^3}e^{-\beta(E_1+E_2)}|\vec{v}_1-\vec{v}_2|, \tag{16}$$

and it is expected to be independent of the microscopic form of the differential cross section. The 1/2 on the right-hand side of Eq. (16) takes into account the two identical incoming particles. The identity of two incoming gluons has been taken into account in the scattering cross section. In Appendix A, we show that the above six-dimensional integral can be reduced to a one-dimensional integral:

$$W=\frac{8T^6}{\pi^3\mu^2}F\left(\frac{2m}{T}\right), \tag{17}$$

in which $F(x)=\int_x^\infty dy y^2(y^2-x^2)K_1(y)$ [13].

III. NUMERICAL TESTS OF THE ZPC MODEL

For the cascade calculations, we take the temperature $T=0.5$, 1, 1.5 GeV, and set the total number of particles in the periodic box to be $N=4000$. The volume is related to the density of particle at zero-chemical potential,

$$\rho=\frac{\gamma}{(2\pi)^3}4\pi\int_0^\infty dp p^2 e^{-\beta E}, \tag{18}$$

via $V=N/\rho$. In ZPC, there are 1000 computation cells of volume $V/1000$. We specify the cell size to the cascade code.

To study the mass dependence, we choose three different masses: 0, 2.5, and 5 GeV. For the dependence on the scattering cross section, the interaction length $\sqrt{\sigma/\pi}=1/\mu$ is set to be 0.5λ, λ, and 1.5λ. In the above λ is a rough estimate for the mean free path

$$\lambda=\frac{1}{\rho\sigma}. \tag{19}$$

We specify the screening mass μ to the cascade code.

The parameters for the cascade measurement are shown in Table I. Unless otherwise stated, we will use the ZPC default scattering scheme, i.e., a collision time is determined in the two colliding particle center-of-mass frame, and the collision space point is the center of the two colliding particle positions in their center-of-mass frame. As we know [11], this scheme is not sensitive to the global frame used to order the collisions. We refer to this scheme as scheme (a) in the following.

Figure 1 shows the pressure-energy density ratio P/ϵ as a function of m/T, and Fig. 2 shows the energy density as a function of temperature T for different particle masses. We see very good agreement between the predictions and the cascade results. This indicates that the initial momentum distributions are correctly generated. There is no time dependence of the pressure and energy density over a time period of 6 fm during which each particle has experienced ~ 10 collisions on average.

TABLE I. Input parameters to ZPC: cell size and screening mass for different temperatures and masses of particles. μ_1, μ_2, μ_3 correspond to three decreasing screening masses as described in the text.

$T=0.5$ GeV	$m=0$ GeV	$m=2.5$ GeV	$m=5$ GeV
l_c (fm)	0.532 405 97	1.315 035 18	5.196 534 01
μ_1 (fm^{-1})	5.501 786 69	2.227 456 82	0.563 680 34
μ_2 (fm^{-1})	4.366 770 96	1.767 933 64	0.447 393 38
μ_3 (fm^{-1})	3.465 908 38	1.403 209 85	0.355 096 36
$T=1.0$ GeV	$m=0$ GeV	$m=2.5$ GeV	$m=5$ GeV
l_c (fm)	0.266 202 98	0.367 664 46	0.657 517 57
μ_1 (fm^{-1})	11.003 573 61	7.967 003 54	4.454 913 73
μ_2 (fm^{-1})	8.733 542 10	6.323 414 86	3.535 867 35
μ_3 (fm^{-1})	6.931 816 91	5.018 897 67	2.806 419 75
$T=1.5$ GeV	$m=0$ GeV	$m=2.5$ GeV	$m=5$ GeV
l_c (fm)	0.177 468 65	0.209 810 78	0.293 208 39
μ_1 (fm^{-1})	16.505 360 62	13.961 075 15	9.990 110 02
μ_2 (fm^{-1})	13.100 313 31	11.080 912 61	7.929 155 53
μ_3 (fm^{-1})	10.397 725 50	8.794 926 11	6.293 374 87

For periodic slab initial conditions, T^{11} evolution at position $L/4$ in the free streaming case is compared with prediction in Fig. 3. Also shown in Fig. 3 is the result (filled circles) with interactions turned on. We see that interactions reduce the rate of collective expansion compared to free streaming and also the oscillations damp faster than in the free streaming case. For the noninteracting free streaming case, good agreement of prediction (dashed line) and cascade results (pluses) is shown for the T^{11} evolution at $L/4$ in Fig. 3 and time evolution of free streaming T^{11} spatial distribution in Fig. 4. Time evolution of free streaming A^{zx} spatial distribution (Fig. 5) also agrees well with the prediction.

Figures 6 and 7 give scaled collision rate per unit volume as a function of m/T. The data points with the same m/T,

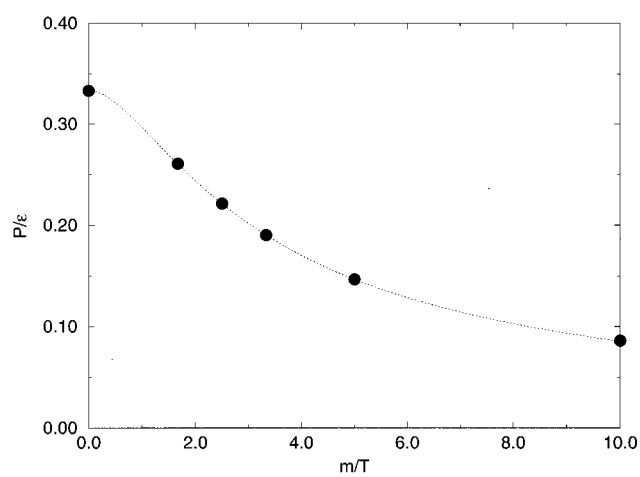

FIG. 1. Pressure-energy density ratio P/ϵ as function of m/T. The dotted curve is the analytic prediction, and the filled black dots are cascade data.

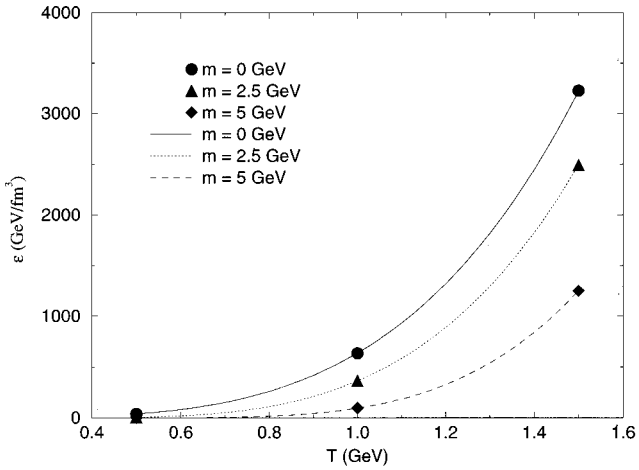

FIG. 2. Energy density ϵ as a function of temperature T for different masses. The curves are predictions, and the dots are cascade data.

and same μ overlap. The three data sets at the same m/T correspond to three different screening masses μ. The smaller the screening mass, the lower the collision rate.

The collision rate is the same for the ZPC default Yukawa-type scattering differential cross section and the straight line propagation. This indicates the collision number loss is not due to particle shielding.

With small screening mass, the interaction range is large. When the interaction range is much larger than the mean free path, noncausal collisions become more abundant. To process the noncausal collision, we pick up one collision out of several collisions for one particle according to the ordering time (see Ref. [11] for details). This process neglects other collisions in the same noncausal collision set. Some of them will not be recovered later. The larger the interaction range, the larger percentage of noncausal collisions. Hence, more collisions are neglected and the collision rate is lower than expected.

In the dilute limit, the percentage of noncausal collisions out of the total number of collisions for massless particles is

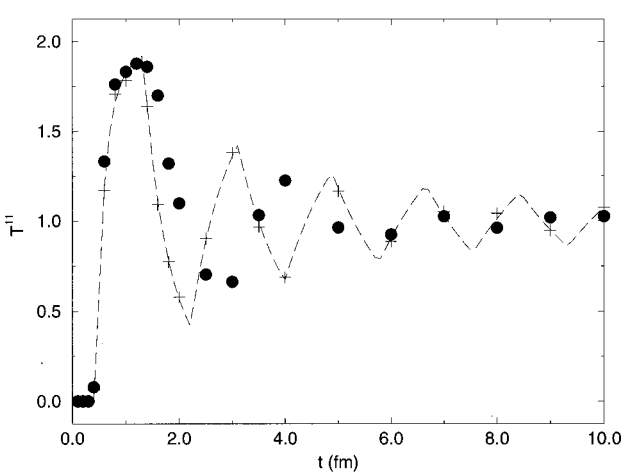

FIG. 3. Evolution of the longitudinal momentum flux. T^{11} is in units of $T^{11}(\infty)$. The size of the box is determined by the asymptotic temperature $T=1.5$ GeV, and the screening mass is set to be 16.5 fm^{-1} for the interacting case.

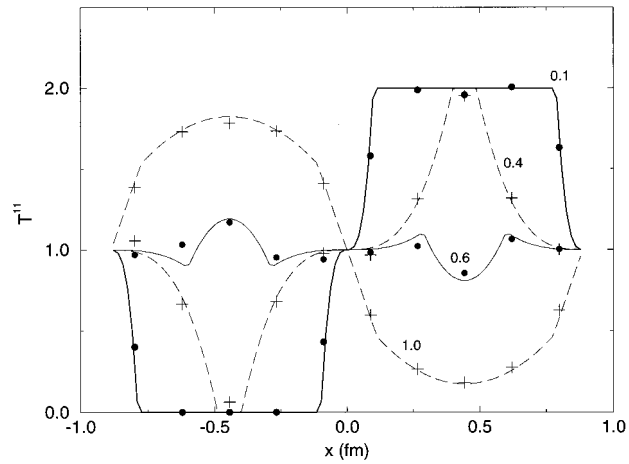

FIG. 4. Evolution of T^{11} spatial distribution. The predictions are drawn with solid and dashed lines alternatively with numbers indicating the times in fm. The cascade data are drawn in filled circles and pluses alternatively for different times. Asymptotic temperature $T=1.5$ GeV.

proportional to the number of particles inside the causal sphere in the two colliding particle center-of-mass frame. The radius of the sphere is proportional to the impact parameter. So

$$\frac{N_{\text{nonc}}}{N_{\text{total}}} \propto \frac{1}{\sigma}\int_0^{\sqrt{\sigma/\pi}} 2\pi b db \frac{4\pi}{3} b^3 \overline{\gamma}\rho = \frac{8}{15}\overline{\gamma}\rho\frac{\sigma^{3/2}}{\sqrt{\pi}}.$$

$2\pi b db/\sigma$ is the probability of having impact parameter b. Here, $\overline{\gamma}$ is for the averaged boost factor from lab frame to the two colliding particle center-of-mass frame. In the case of massless particles, $\overline{\gamma}\approx 2$. $4\pi b^3\overline{\gamma}\rho/3$ gives the number of particles in the sphere with radius b in the two colliding particle center-of-mass frame. The exact radius of the sphere depends on the definition of noncausal collisions [1,11] and the collision prescription of cascade.

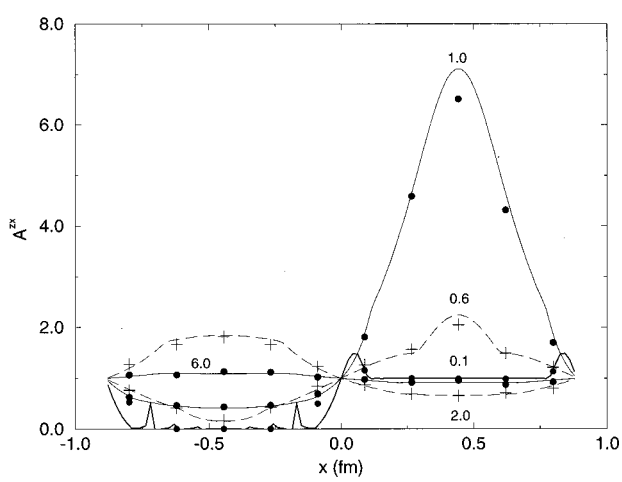

FIG. 5. Evolution of A^{zx} spatial distribution. The predictions are drawn with solid and dashed lines alternatively with numbers indicating the times in fm. The cascade data are drawn in filled circles and pluses alternatively for different times. Asymptotic temperature $T=1.5$ GeV.

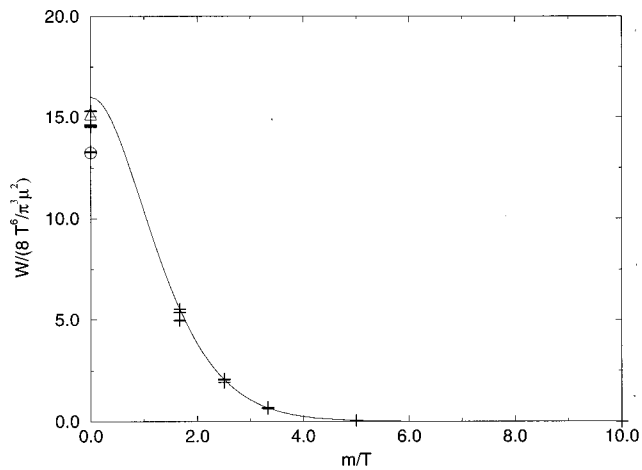

FIG. 6. Collision rate per unit volume W as a function of m/T. The curve is the prediction, and the pluses are cascade data. The open circle corresponds to the rate at $m/T=0$ with $\mu=3.465\,908\,38$ fm^{-1}. The result from scaling the cross section down by a factor of 10 and increasing the particle density by a factor of 10 is shown as the open triangle.

The noncausal to total ratio is closely related to the ratio of interaction length to the mean free path:

$$\chi=\frac{\sqrt{\sigma/\pi}}{1/\rho\sigma}=\rho\frac{\sigma^{3/2}}{\sqrt{\pi}}.$$

We see $N_{\rm nonc}/N_{\rm total}$ decreases linearly with χ as $\chi\rightarrow 0$. This motivates the algorithm of reducing the noncausal collision percentage [1] by subdividing the particles by a factor l so that $\rho\rightarrow l\rho$ while decreasing $\sigma\rightarrow\sigma/l$. This preserves the mean free path $1/\sigma\rho$ while $\chi\propto 1/\sqrt{l}\rightarrow 0$.

To study the noncausal collisions, it is easy to use the two particle center-of-mass scattering scheme with collision position for each particle taken as the position of the particle at the collision time in the two particle center-of-mass frame [scheme (b)]. The number of noncausal collisions, and total number of collisions for 4000 particles with $m=0$, $T=0.5$ GeV, and a time period of 6 fm is summarized in Table II. In the table, μ is the screening mass. a gives the ratio of interaction length to the estimate of mean free path before rescaling. l is the scaling parameter, i.e., the total number of particles is increased by a factor of l and the cross section is decreased by a factor of l (but the number of collisions is still for 4000 particles). χ_1 is the ratio of interaction length to the estimate of mean free path including the rescaling, i.e., $\chi_1=a/\sqrt{l}$. χ_2 is the ratio of interaction length to the measured mean free path. The mean free path is measured through the formula, $\rho/(2W)$, in which W is the collision rate per unit volume and the particles are moving at the speed of light. The ratio of the number of noncausal collisions to the total number of collisions is also plotted in Fig. 8 against the ratio of interaction length to the mean free path. In Fig. 8, the open circles are data against χ_1 and the filled circles are against χ_2. It shows that when the density increases, i.e., when χ increases, the difference between χ_2 and χ_1 increases. This tells us that when density is high, the naive formula for the estimate of mean free path, $\lambda=1/(\rho\sigma)$, needs to be corrected. Also we see the data deviate from linear formula and has a tendency of saturation when density is large. This is consistent with the fact that the ratio should always be less than 50% from the definition of the noncausal collision.

When we fix μ and increase l from 1 to 5, the total number of collisions goes up from 64 700 for $l=1$ to 75 400 for $l=5$. For $l=10$, the total number of collisions is 77 800. We see clearly the trend toward a constant value of total number of collisions when l is increased. In scheme (a), there

TABLE II. Measurement of noncausal collision number and total collision number.

μ (fm^{-1})	a	l	χ_1	χ_2	$N_{\rm nonc}$	$N_{\rm total}$	R
5.501 786 69	0.5	1	0.5	0.48	3240	31400	10.3%
4.366 770 96	1	1	1	0.88	8250	46100	17.9%
3.465 908 38	2	1	2	1.56	19000	64700	29.4%
3.465 908 38	2	5	0.89	0.81	12500	75400	16.6%
3.465 908 38	2	10	0.63	0.59	9700	77800	12.5%

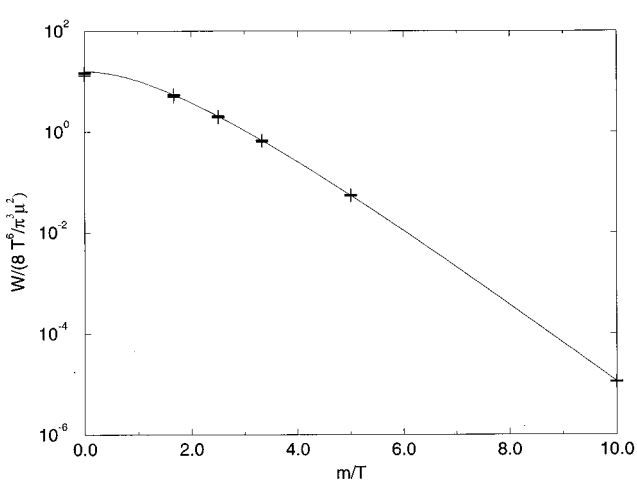

FIG. 7. Collision rate per unit volume W as a function of m/T. The curve is the prediction, and the pluses are cascade data.

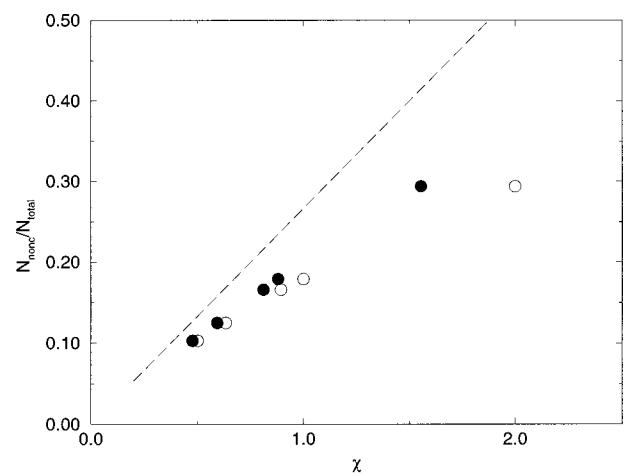

FIG. 8. The number of noncausal collisions over the total number of collisions as a function of the ratio of interaction length to the mean free path. The dashed curve is the estimate when the radius of causal sphere is taken to be the interaction range. Open (filled) circles are data plotted against χ_1 (χ_2) in Table II.

are 70 000, 78 000, and 80 000 collisions for $l=1$, 5, 10, respectively. Scheme (a) collision rate with $l=10$ is shown in Fig. 6 as an open triangle (the $l=1$ data is shown as an open circle). The data show that particle partition improves the cascade result. In addition, we observe that scheme (a) collision rate is always higher than that of scheme (b). The closer the cascade rate is to the analytic prediction, the smaller the percentage difference. In this sense, the percentage difference of cascade results from different schemes can be used as an indicator of the cascade systematic errors.

During the preliminary study of the collision rate, we found when $m/T=10$, the collision rate is higher than the predicted rate. By looking more carefully into the code, we found out that it was caused by the larger than statistical fluctuations in the position distribution. When the fugacity λ is not uniform in space, the collision rate per unit volume:

$$W=\int \frac{d^3x}{V}\lambda^2(x)I, \tag{20}$$

in which

$$I=\frac{\pi}{\mu^2}\gamma^2\int \frac{d^3p_1}{(2\pi)^3}\frac{d^3p_2}{(2\pi)^3}e^{-\beta(E_1+E_2)}|\vec{v}_1-\vec{v}_2|. \tag{21}$$

By using the inequality,

$$\int \frac{d^3x}{V}\lambda^2(x)\geqslant\left(\int \frac{d^3x}{V}\lambda(x)\right)^2, \tag{22}$$

and the fact that the system we prepared has zero chemical potential and hence averaged fugacity is one, we arrive at

$$W\geqslant W_0=\frac{\pi}{\mu^2}\gamma^2\int \frac{d^3p_1}{(2\pi)^3}\frac{d^3p_2}{(2\pi)^3}e^{-\beta(E_1+E_2)}|\vec{v}_1-\vec{v}_2|. \tag{23}$$

The equality holds only when the fugacity has no spatial dependence. This shows that when there are space clusters existing for some time period, the collision rate is higher than that expected for the uniform system.

It was found only in $m/T=10$ and not in other cases because in the $m/T=10$ case, particles are moving very slowly, and they stay in clusters for a much longer time.

We traced the origin of the nonuniform distribution. It was caused by some correlation of random number generators (see Appendix B). When we use ran1 from [14], and generate first the momenta for all the particles and then generate the positions for all the particles, there are no abnormal fluctuations. When we generate momentum and position together, we found abnormal fluctuations. This does not occur when ran3 from [14] is used. We correct the generation by separating the generation of particle momentum and particle position [15].

IV. CONCLUSIONS

From the above study, we show that the equation of state and the collision rate can be used to test the initial conditions and collision mechanisms of relativistic parton cascade. It is important to notice that for massless particles, when the interaction range is larger than the mean free path, the cascade collision rate is significantly lower than the theoretical value. This gives rise to systematic errors of parton cascade simulations. Other methods, e.g., particle partition, have to be used to correct the collision rate.

The comparison of free streaming and the interacting cascade approach to equilibrium indicate qualitative similarities of the two cases. However, the damping and speed of collective motion are quite different. A detailed comparison of free streaming, ideal hydrodynamics, and cascade approach to global equilibrium in the case of half-filled periodic box initial conditions will be addressed in another paper [16].

As discussed in this paper, spatial distribution with larger than statistical fluctuations gives higher than thermal reaction rate. HIJING [17] predicts initial spatial clusters of partons for nucleus-nucleus collisions at collider energies. This implies higher than thermal collision rates [18] and many other interesting physical phenomena beyond the widely used hot gluon scenario [19] predictions.

We emphasize the importance of using analytic tests in debugging numerical simulation codes. The spatial distribution with abnormal fluctuations illustrates well the usefulness of the analytic collision rate test. As more components are added to the cascade code, more tests will be needed to ensure the consistency of different parts of the cascade code and to enable disentangling of the actual physical assumptions that define the model.

ACKNOWLEDGMENTS

We thank S. A. Chin, P. Danielewicz, V. Koch, B. A. Li, S. Pratt, and J. Randrup for useful discussions. We also thank Brookhaven National Laboratory and Lawrence Berkeley Laboratory for providing computing facilities. This research was supported by the U.S. Department of Energy under Contract No. DE-FG02-93ER40764. Y. Pang was partially supported by the U.S. Department of Energy Grant No. DE-FG02-92ER40699, DE-AC02-76CH00016, and the Alfred P. Sloan Foundation.

APPENDIX A: REDUCTION OF THE PHASE SPACE INTEGRAL IN THE COLLISION RATE CALCULATION

To calculate the collision rate per unit volume, Eq. (16), we first replace $|\vec{v}_1-\vec{v}_2|$ by

$$\frac{\sqrt{s(s-4m^2)}}{2E_1E_2},$$

and get

$$W=\frac{1}{2}\frac{2\pi}{\mu^2}\gamma^2\int_{4m^2}^{\infty}ds\sqrt{s(s-4m^2)}\int \frac{d^3p_1}{(2\pi)^3 2E_1}\frac{d^3p_2}{(2\pi)^3 2E_2}\times e^{-\beta(E_1+E_2)}\delta(s-(p_1+p_2)^2). \tag{A1}$$

The δ function can be used to integrate out one angle by using:

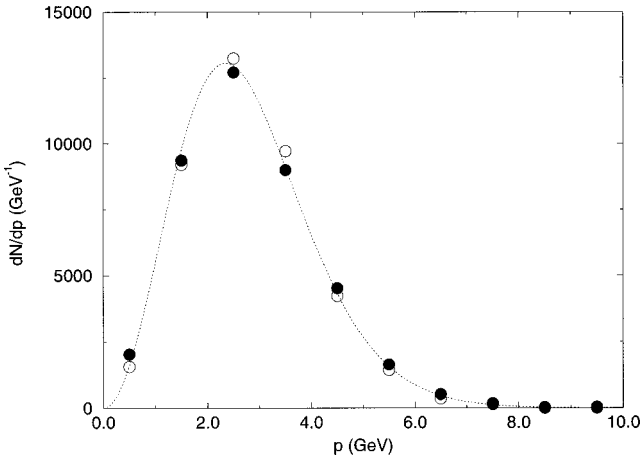

FIG. 9. Momentum distribution for $m=5$ GeV, $T=0.5$ GeV with 40 000 particles. The dotted line is the prediction, the open circles come from code using ran1, and the filled circles are ran3 results.

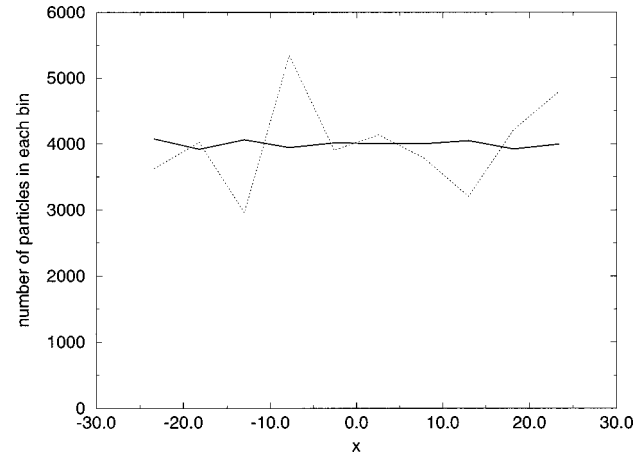

FIG. 10. Number of particles per bin as a function of position x for $m=5$ GeV, $T=0.5$ GeV with 40 000 particles. The dotted curve is ran1 result, while the solid curve is for ran3.

$$\delta(s-(p_1+p_2)^2)=\frac{1}{2p_1p_2}\delta\left(\cos\ \theta_2+\frac{s-2m^2-2E_1E_2}{2p_1p_2}\right). \tag{A2}$$

After carrying out the angular integrals, the collision rate becomes

$$W=\frac{\pi\gamma^2}{4(2\pi)^6\mu^2}\int_{4m^2}^{\infty}ds\sqrt{s(s-4m^2)}\frac{4\pi p_1^2dp_1\ 2\pi p_2^2dp_2}{E_1E_2\ 2p_1p_2}$$
$$\times e^{-\beta(E_1+E_2)}\Theta\left(1-\left|\frac{s-2m^2-2E_1E_2}{2p_1p_2}\right|\right). \tag{A3}$$

The Θ function constraint can be written as

$$(E_1+E_2)^2m^2<sE_1E_2+m^2s-\frac{s^2}{4}.$$

Now we change integration variables from E_1, E_2 to $x=E_1E_2$, and $y=E_1+E_2$. The collision rate becomes

$$W=\frac{\pi\gamma^2}{2(2\pi)^4\mu^2}\int_{4m^2}^{\infty}ds\sqrt{s(s-4m^2)}$$
$$\times\int dxdy\frac{e^{-y/T}}{\sqrt{y^2-4x}}\Theta\left(x+m^2-\frac{s}{4}-\frac{y^2m^2}{s}\right). \tag{A4}$$

The integration over x can be carried out first. The absolute lower bound of $x=E_1E_2$ is m^2, but x is also restricted by the Θ function. By noticing $y\geqslant s$, and hence $y^2m^2/s-m^2+s/4>m^2$, we see the lower bound should be $y^2m^2/s-m^2+s/4$. The upper bound is determined from the square root in the integrand to be $y^2/4$. The result is

$$\int_{y^2m^2/s-m^2+s/4}^{y^2/4}dx\frac{1}{\sqrt{y^2-4x}}=\frac{1}{2}\sqrt{(s-4m^2)(y^2/s-1)}. \tag{A5}$$

Now the collision rate per unit volume is reduced to a two-dimensional integral:

$$W=\frac{\pi\gamma^2}{4(2\pi)^4\mu^2}\int_{4m^2}^{\infty}ds(s-4m^2)\int_{\sqrt{s}}^{\infty}dye^{-y/T}\sqrt{y^2-s}. \tag{A6}$$

The y integral can be readily carried out to be

$$\int_{\sqrt{s}}^{\infty}dye^{-y/T}\sqrt{y^2-s}=\sqrt{s}TK_1\left(\frac{\sqrt{s}}{T}\right). \tag{A7}$$

In the above, $K_1(x)$ is the modified Bessel function. Taking $\gamma=16$, we arrive at Eq. (17).

APPENDIX B: ONE EXAMPLE SHOWING THE INTERFERENCE OF GENERATIONS OF DISTRIBUTIONS OF VARIABLES

The following is a sample program that generates the particle momentum and position together. ran1 is taken from [14] and declared as a real*8 function.

```
program dist
implicit real*8 (a-h, o-z)
parameter (mul = 40000)
parameter (size = 5.19653401d0)
external ran1
common /para/ xmp
temp = 0.5d0
xmp = 5d0
do i = 1, mul
   call energy(e, temp)
   call momentum(px, py, pz, e)
   x = 2d0 * ran1(iseed) - 1d0
   x = x * 5d0 * size
   y = 2d0 * ran1(iseed) - 1d0
   y = y * 5d0 * size
   z = 2d0 * ran1(iseed) - 1d0
   z = z * 5d0 * size
end do
stop
end

subroutine energy(e, temp)
implicit real*8 (a-h, o-z)
```

```
  external ran1
  common /para/ xmp
1000 continue
  e = ran1(iseed)
  e = e * ran1(iseed)
  e = e * ran1(iseed)
  if (e .le. 0d0) goto 1000
  e = - temp * log(e)
  if (ran1(iseed) .gt. exp((e - sqrt(
  & e ** 2 + xmp ** 2))/temp)) then
    goto 1000
  end if
  return
  end

  subroutine momentum(px, py, pz, e)
  implicit real*8 (a-h,o-z)
  external ran1
  parameter (pi = 3.14159265358979d0)
  cost = 2d0 * ran1(iseed) - 1d0
  sint = sqrt(1d0 - cost ** 2)
  phi = 2d0 * pi * ran1(iseed)
  px = e * sint * cos(phi)
  py = e * sint * sin(phi)
  pz = e * cost
  return
  end
```

The momentum distribution is shown in Fig. 9 along with that generated by ran3, and the theory prediction. We see that the momentum distribution is correctly generated with reasonable fluctuations.

Figure 10 gives the position x distribution from the above program using ran1 and ran3. The ran1 result has much larger fluctuations than the expected statistical fluctuations, while the ran3 result is consistent with the expected statistical fluctuations.

When the generation of momentum and position are separated, the distributions all have reasonable fluctuations. Another possible (and more efficient) way to solve the problem is to generate Gaussian momentum distribution for large m/T values.

Since with the above program, the total number of random numbers used is 141 931 896, while we can easily show the period of ran1 with the given parameters is beyond 2 000 000 000, it is not clear that the large fluctuations are due to the period of the random number generator ran1. But this is a concrete example of ill-generated distribution.

[1] Y. Pang, GCP, *http://rhic.phys.columbia.edu/rhic/gcp*; Proceedings of RHIC'96, CU-TP-815.

[2] Klaus Werner, VENUS, *http://www-subatech.in2p3.fr/ Sciences/ Theorie/venus/venus.html*; Phys. Rep. **232**, 87 (1993).

[3] Klaus Kinder Geiger, *http://rhic.phys.columbia.edu/rhic/vni*; Comput. Phys. Commun. **104**, 70 (1997).

[4] Bin Zhang, ZPC, *http://nt1.phys.columbia.edu/people/bzhang/ ZPC/zpc.html*; Comput. Phys. Commun. **109**, 193 (1998).

[5] G. Welke, R. Malfliet, C. Grégoire, and M. Prakash, Phys. Rev. C **40**, 2611 (1989).

[6] D. Rischke, S. Bernard, and J. A. Maruhn, Nucl. Phys. **A595**, 346 (1995).

[7] D. Rischke, Y. Pürsün, and J. A. Maruhn, Nucl. Phys. **A595**, 383 (1995).

[8] http://rhic.phys.columbia.edu/oscar/

[9] M. Gyulassy, Y. Pang, and B. Zhang, Nucl. Phys. **A626**, 999 (1997).

[10] G. Kortemeyer, W. Bauer, K. Haglin, J. Murray, and S. Pratt, Phys. Rev. C **52**, 2714 (1995).

[11] B. Zhang and Y. Pang, Phys. Rev. C **56**, 2185 (1997).

[12] W. Greiner, L. Neise, and H. Stöcker, *Thermodynamics and Statistical Mechanics* (Verrlag Harri Deutsch, Frankfurt am Main, 1987).

[13] See, e.g., J. Rafelski and B. Müller, Phys. Rev. Lett. **48**, 1066 (1982); T. S. Biró, P. Lévai, and B. Müller, Phys. Rev. D **42**, 3078 (1990), for similar expressions.

[14] W. H. Press, B. P. Flannery, S. A. Teukolsky, and W. T. Vetterling, *Numerical Recipes: the Art of Scientific Computing* (Cambridge University Press, Cambridge, 1986), Chap. 7.

[15] See, e.g., I. Vattulainen, T. Ala-Nissila, and K. Kankaala, Phys. Rev. Lett. **73**, 2513 (1994), and references therein, for more examples and tests of pseudorandom number generators.

[16] M. Gyulassy, D. Rischke, and B. Zhang (unpublished).

[17] X. N. Wang and M. Gyulassy, Phys. Rev. D **44**, 3501 (1991); M. Gyulassy and X. N. Wang, Comput. Phys. Commun. **83**, 307 (1994).

[18] M. Gyulassy, D. Rischke, and B. Zhang, Nucl. Phys. **A613**, 397 (1997).

[19] E. Shuryak, Phys. Rev. Lett. **68**, 3270 (1992).